Catalytic Ammonia Decomposition Over Ruthenium Nanoparticles Supported on Nano-Titanates

Asbjørn Klerke · Søren Kegnæs Klitgaard · Rasmus Fehrmann

Abstract Nanosized $Na_2Ti_3O_7$, $K_2Ti_6O_{13}$ and $Cs_2Ti_6O_{13}$ materials were prepared and used as supports of ruthenium nanoparticles for catalytic ammonia decomposition. It is shown that these catalysts exhibit higher catalytic activity than ruthenium supported on TiO_2 nanoparticles promoted with cesium. The difference is attributed to the use of nanostructured materials with incorporated alkali metals in the crystal lattice, which apparently gives a higher effect of the promoter. All samples were characterized by X-ray powder diffraction, transmission electron microscopy and N_2 physisorption measurements. Furthermore, the effect of ruthenium loading on the catalytic decomposition of ammonia was investigated.

Keywords Ammonia decomposition ·
Ruthenium nanoparticles · Titanate nanowires ·
Titanate nanotubes · Hydrogen production

1 Introduction

In the past decades, the increased CO_2-emission to the atmosphere from utilization of fossil fuels has led to intensive research in order to substitute the fossil resources, like oil and coal, with suitable alternatives. One of the more promising ideas is to use hydrogen as energy carrier [1–3]. The hydrogen economy has come far but the final breakthroughs regarding some of the major challenges are still to come. The challenge of how to store and transport hydrogen efficiently has led to an increased interest in using various materials for direct hydrogen storage [4–10]. All of those technologies are still only at the research stage and far from widespread commercial use. The challenge of how hydrogen can be produced in a cheap, efficient and "green" way has also achieved attention in several studies [11–15], but most hydrogen is still produced from methane by steam-reforming and the water gas shift reaction. The efficient conversion of hydrogen into electricity is the only technology that is now starting to get commercialised and several operational hydrogen fuel cell systems are now available on the market (http://www.ballard.com/, http://www.dantherm-power.com/).

The lack of a significant breakthroughs for direct hydrogen storage has led to increased interest in indirect hydrogen storage, e.g., in methanol, ethanol and methane [16, 17], but all these compounds contain carbon and will unavoidably produce CO_2 at the end user. Therefore, ammonia as an indirect hydrogen storage medium has gained renewed focus [18–20]. The main reason for this interest is that ammonia is a bulk chemical that is widely available and has a high hydrogen density on both weight and volume bases [21]. Ammonia can also be transported and stored as a liquid by known and well-proven technology [22]. Moreover, the use of ammonia as an indirect hydrogen storage media has been promoted by the development of efficient and reversible solid ammonia storage in the form of metal ammines [23]. Metal ammines make the use of ammonia safe by lowering the vapor pressure [24]. However, the use of ammonia as an indirect hydrogen source makes it necessary to perform a catalytic decomposition of ammonia to liberate nitrogen and hydrogen.

The ammonia decomposition reaction has traditionally been studied to gain more information about the ammonia synthesis catalyst [25]. This is, however, changing as

A. Klerke · S. K. Klitgaard · R. Fehrmann (✉)
Centre for Catalysis and Sustainable Chemistry, Department of Chemistry, Technical University of Denmark, Building 206, 2800 Lyngby, Denmark
e-mail: rf@kemi.dtu.dk

ammonia is getting more attention as a potential hydrogen carrier. Several studies have shown that ammonia can easily be decomposed to CO_x-free hydrogen [26–28]. Furthermore, studies of the optimal catalyst for the ammonia decomposition reaction have shown that ruthenium nanoparticles promoted with cesium and supported on graphitized carbon is the currently best catalyst candidate [29–31]. The general trend for the effect of the alkali metal promoters on ruthenium catalysts for ammonia decomposition has also been studied and found to be Cs > K > Na > Li [32].

In this paper, we investigate how nanostructured titanates with incorporated alkali metals, can be used as combined supports and promoters for ruthenium catalysts in the ammonia decomposition reaction. The idea is that by incorporating the promoter into the support material, the promoter will be better dispersed or activated in the crystal lattice and thereby increase the promoting effect. Furthermore, the nanostructured supports will give higher surface area, which is also expected to increase the activity.

The support materials are characterized by X-ray powder diffraction (XRPD), transmission electron microscopy (TEM) and N_2 physisorption measurements. The XRPD is done to verify that the synthesis of the support materials is complete, and no TiO_2-phase is present. TEM is used to evaluate the detailed nanostructure of the support materials and the physisorption is done to evaluate the total surface areas of the different support materials. After the catalyst is prepared the apparent particle size of ruthenium is tested with pulse chemisorptions under similar reduction conditions to those applied under the final catalyst testing. The final catalysts are tested for catalytic activity in the ammonia decomposition reaction.

2 Experimental

2.1 Catalyst Preparation

2.1.1 Synthesis of Alkaline Titanate Nanomaterial Supports

Alkaline nanostructured titanates were prepared by hydrothermal treatment of TiO_2 with different alkaline bases. The hydrothermal treatment of TiO_2 was done with NaOH (Sigma–Aldrich 98%), KOH (Sigma–Aldrich 90%), and $CsOH \cdot H_2O$ (Sigma–Aldrich, Cabot high-purity grade) giving the corresponding alkaline titanate nanostructures: sodium titanates $Na_2Ti_3O_7$ nanotubes, potassium titanates $K_2Ti_6O_{13}$ nanowires and cesium titanates $Cs_2Ti_6O_{13}$ nanowires [33–35]. The produced materials were then used as supports for ruthenium nanoparticles.

In a typical synthesis of the alkaline titanate nanomaterials, 1.92 g of the commercial TiO_2 anatase nanoparticles were suspended in 160 mL of aqueous 10 M alkaline base, followed by hydrothermal treatment at 150 °C in a stainless Teflon-lined autoclave for 72 h. The resulting powders were washed with large amounts of distilled water until neutral pH was achieved and dried at room temperature.

2.1.2 Preparation of Ruthenium Nanoparticles

The catalysts were prepared from 0.5 g of the titanate nanostructured material by incipient wetness impregnation using a ruthenium nitrosyl nitrate solution with a ruthenium content of 8.1 wt%. After impregnation, the sample was calcined in air at 250 °C.

2.2 Physicochemical Characterization

2.2.1 Transmission Electron Microscopy

Transmission electron microscopy was performed on a JEM 2000 FX with an accelerating voltage of 300 kV. A few milligram of the powdered samples were suspended in 2 mL ethanol, and the suspension was sonicated for 30 min. The suspension was allowed to settle for 15 min, before a drop was taken and dispersed on a 300 mesh copper grid coated with Holey carbon film.

2.2.2 X-Ray Powder Diffraction

X-ray powder diffraction patterns were recorded using Cu-K$_\alpha$ radiation in the 2θ interval of 5–100° by a Philips PW 1820/3711 powder diffractometer.

2.2.3 Nitrogen Adsorption and Desorption

Nitrogen adsorption and desorption measurements were performed at liquid nitrogen temperature on a Micromeretics ASAP 2020. The samples were outgassed in vacuum at 200 °C prior to measurement. Total surface areas were calculated according to the BET method.

2.2.4 CO-Pulse Chemisorption

CO-pulse chemisorption was performed on the same catalyst batch used for activity testing. The CO-pulse chemisorption was done on a Micromeretics Auto Chem II chemisorption analyzer. A sample of 0.1 g catalyst was reduced in hydrogen for 2 h at 400 °C, then the gas was switched to helium for 1 h before the sample was cooled in a flow of helium to 50 °C and pulsed with 5% CO in

helium. From the amount of adsorbed CO the apparent particle size was calculated.

2.3 Catalyst Testing

The catalyst testing was performed in a specialized setup for ammonia decomposition. 0.1 g of catalyst was transferred to the stainless steel reactor with an inner diameter of 4.6 mm, where it was reduced for 5 h at 400 °C in a 100 mL/min flow of hydrogen. The temperature of 400 °C for reduction in all experiments is selected to avoid decomposition of the alkali nano-titanate supports. The decomposition of the supports was observed in catalytic testing at 490 °C as a rapid deactivation of the catalysts and can be due to ammonia or hydrogen destabilizing the nanostructure at high temperatures. The temperature can influence the degree of reduction; if the reduction is not complete the measured apparent particle size will increase. The testing was done from 400 °C and down using steps of 15 °C in a flow of 20 mL/min ammonia and 50 mL/min argon. The ammonia concentration in the carrier stream was determined using a Fischer–Rosemount NGA 2000 equipped with a MLT analyzer calibrated to NH_3 concentrations from 0.03 to 30%.

3 Results and Discussion

3.1 Characterisation

The prepared titanate nanostructured support materials were analysed with high-resolution TEM. Representative TEM images of the titanate nanomaterials can be seen in Fig. 1.

In Fig. 1a, the TiO_2 anatase nanoparticles used as starting material for the synthesis of the alkaline titanate nanomaterials are shown. The results of the hydrothermal treatments of TiO_2 anatase nanoparticles with different alkaline bases, NaOH, KOH, and CsOH, are shown in Fig. 1b, c and d, respectively. From the TEM images, is it seen that the hydrothermal treatment gives nanotubes in the case of NaOH, whereas the use of KOH or CsOH gives small flakes/nanowires.

Fig. 1 TEM images of **a** TiO_2 nanoparticles, **b** $Na_2Ti_3O_7$ nanotubes, **c** $K_2Ti_6O_{13}$ nanowires and **d** $Cs_2Ti_6O_{13}$ nanowires
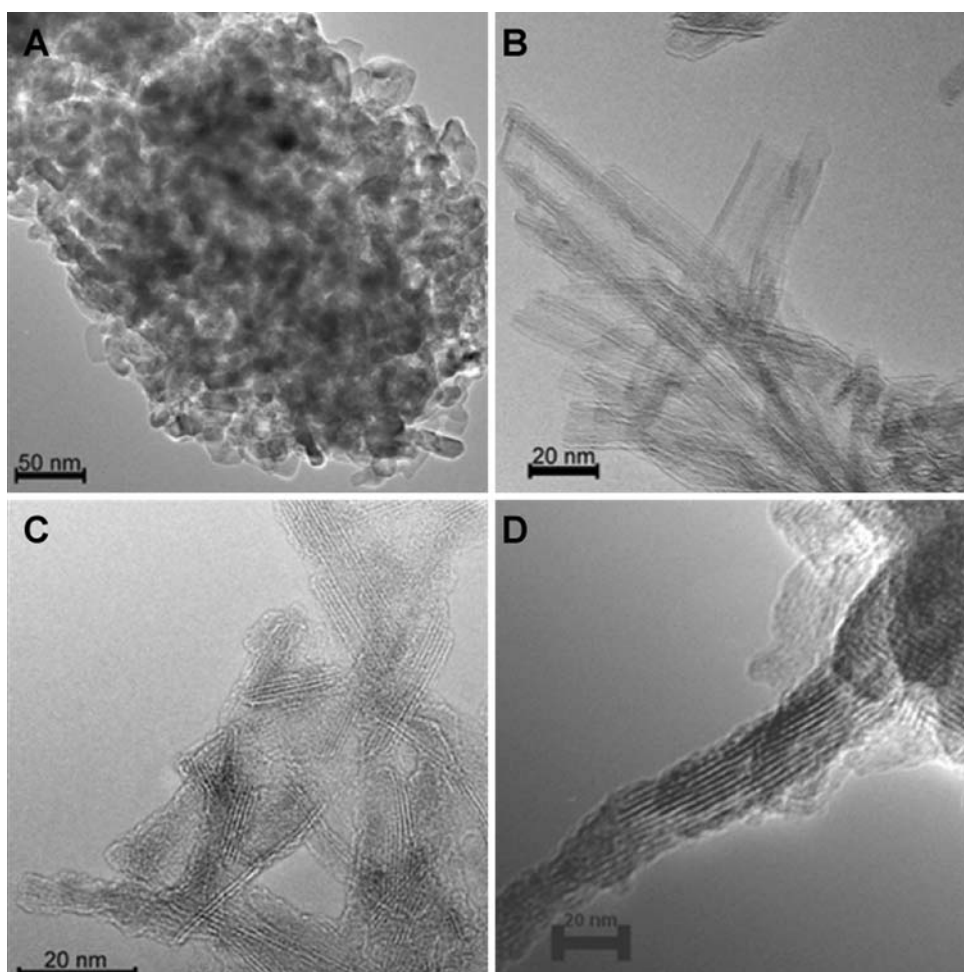
Table 1 BET surface areas of anatase TiO_2 before and after hydrothermal treatment with different alkaline bases

Main product	BET surface area (m^2/g)	Base (M)	Time (h)	Temperature (°C)
TiO_2	139	–	0	–
$Na_2Ti_3O_7$	224	NaOH	72	150
$K_2Ti_6O_{13}$	309	KOH	72	150
$Cs_2Ti_6O_{13}$	208	$CsOH \cdot H_2O$	72	150

Table 1 shows the BET surface areas of samples obtained after hydrothermal treatment with different alkaline bases. From Table 1, it is seen that the surface areas of the nanostructured titanates increase significantly after the hydrothermal treatments with the different alkaline bases in comparison with the starting anatase TiO_2.
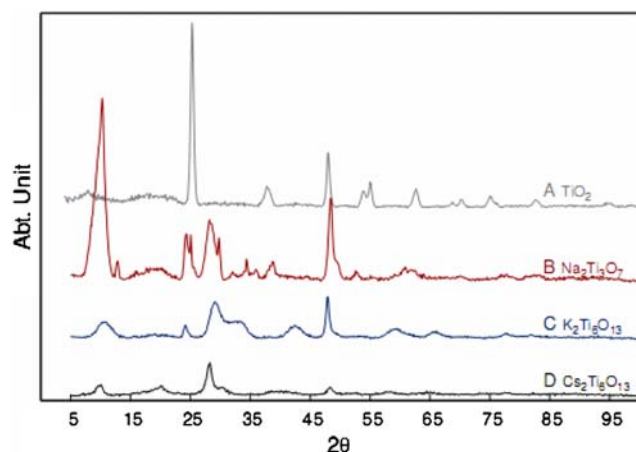
The support materials were also investigated using XRPD. The obtained XRPD-patterns for all the nanomaterial samples are shown in Fig. 2.

The XRPD patterns were obtained in the interval from 5 to 100 (2θ) degrees. XRPD patterns for nanostructured titanates were obtained after hydrothermal treatment. Figure 2A shows crystalline TiO_2 anatase. The other nanomaterials appear less crystalline but this is only because the nanotubes and nanowires are too thin to yield good diffraction. Thus, it is concluded that all the titanium in the samples is present as nanostructured titanate materials and that no TiO_2 nanoparticles are present.

The obtained XRPD patterns are very similar to those previously published for $Na_2Ti_3O_7$ nanotubes [36], $K_2Ti_6O_{13}$ nanowires [37] and $Cs_2Ti_6O_{13}$ nanowires [38, 39].

3.2 Catalyst Testing

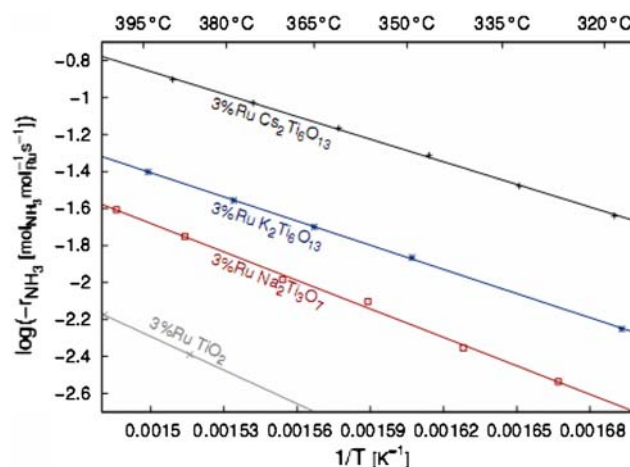All catalysts were tested under the same conditions in a constant flow of ammonia diluted with argon as described in the experimental section. In Fig. 3, an Arrhenius type plot showing the catalytic rate based on active metal concentration of 3% ruthenium on TiO_2 nanoparticles, $Na_2Ti_3O_7$ nanotubes, $K_2Ti_6O_{13}$ and $Cs_2Ti_6O_{13}$ nanowires is given. This confirms the general trend for promotion of ruthenium catalysts with different alkali metals in the ammonia decomposition reaction [32, 40–42].

From Fig. 3, it is seen that the promoting effect of alkali metals increases in the order: Cs > K > Na. To verify that the higher catalytic activity of $Cs_2Ti_6O_{13}$ nanowires was due to structural changes, the ruthenium on TiO_2 support was promoted with a similar cesium loading(~ 30 wt%) using a $CsNO_3$ solution. The promoter was deposited on the already prepared 3% Ru TiO_2 with incipient wetness impregnation, calcined, and tested (not shown), but it showed lower activity than the pure ruthenium on TiO_2. This shows that incorporating alkali metal promoters into the crystal lattice of the nano-titanates, gives a stronger promoting effect than surface deposition of the promoter on top of the ruthenium. The lower activity after promotion has not been seen in other studies were high cesium loadings has been impregnated on a ruthenium catalyst [29, 32, 43].

The relatively high catalytic activity of ruthenium on the nano-titanates can thus be explained by the promoting effect of the alkali metals in the crystal lattice. Furthermore the higher surface area of the alkali titanates will increase the dispersion of the Ru-nanoparticles on the surface.

To further investigate the effect of the $Cs_2Ti_6O_{13}$ support material, samples with different ruthenium loadings were prepared, in order to find the optimum ruthenium content. The effect of varying the ruthenium loading is shown in Fig. 4, the rates are plotted at 377 °C.

Fig. 2 XRPD patterns of (A) TiO_2 nanoparticles, (B) $Na_2Ti_3O_7$ nanotubes, (C) $K_2Ti_6O_{13}$ nanowires and (D) $Cs_2Ti_6O_{13}$ nanowires

Fig. 3 Arrhenius type plot for catalytic ammonia decomposition with 3 wt% ruthenium, respectively, on TiO_2 nanoparticles, $Na_2Ti_3O_7$ nanotubes, $K_2Ti_6O_{13}$ and $Cs_2Ti_6O_{13}$ nanowires as support materials
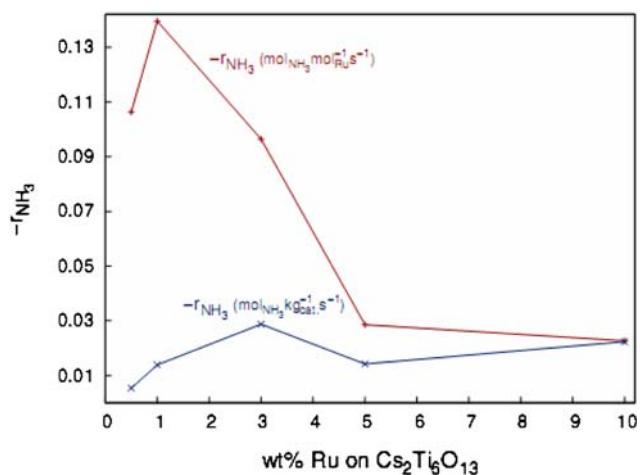
Fig. 4 Reaction rate at 377 °C plotted as a function of the ruthenium loading in wt%. The rates are normalised to molar ruthenium loading (*red*) and catalyst weight (*blue*)

Table 2 Measured particle sizes and molar ratios between cesium and ruthenium in the different catalysts for the same catalyst batches as used for activity measurements in Fig. 4

Wt% Ru $Cs_2Ti_6O_{13}$	Apparent particle size (nm)	Molar ratio Cs/Ru
0.5%	26.0	52.6
1%	7.8	26.2
3%	23.6	8.5
5%	–	5.0
10%	28.6	2.4

The two plots in Fig. 4 illustrate that different normalizing factors is important for understanding the data. For the weight based normalization the normalization factor is constant as all test is done with same amount of catalyst (0.1 g). For normalization to molar ruthenium content the normalization factor changes with a factor of 20 from 0.05 to 0.99 mmol/g. This favours low loading best seen with a comparison between 1 and 5 wt% ruthenium. The two catalysts have similar rates on weight base but on mole base the five times higher Ru-loading of 5 wt% sample gives a rate on mole base that is one-fifth of the 1 wt% sample.

From Fig. 4, it is seen that the best utilization of the available ruthenium on a molar base is achieved with a loading of 1 wt%. The reaction rate also show that the activity per mole ruthenium decreases until a loading of 5 wt% is reached, here after the activity stabilizes. However, the change in specific activity as a function of ruthenium loading is almost invariant, the main features being a lower spread in activity and a shift of the maximum activity to a loading of 3 wt% ruthenium. This is interesting regarding catalyst mass optimization.

The change in activity can partly be explained by different particle sizes, which were measured by CO-chemisorption, see Table 2.

By comparison of the particle size and activity normalised to the ruthenium amount in mole, it is seen that there is a good correlation between the measured particle size and the relative activity. The loading of 1% ruthenium has the highest activity and the lowest particle size. We have no experimental explanation of the observed lower particle size of this catalyst compared to the others displayed in Table 2. The 0.5 and 3% ruthenium loadings have particle sizes and activities in the same ranges. The 10% ruthenium

loading have the highest measured particle size and lowest activity. This is, however, not the full picture, as the particle size for the 10% ruthenium is only slightly larger than for the 3% ruthenium. This indicates that the ratio between cesium and ruthenium also has influence on the measured activity.

Thus, if we look at the particle size and activity for 0.5, 3, and 10% ruthenium, the particle size is in the same range and should not result in large differences in activity due to changes in particle size. This tells us that the cesium loading is also important for the activity and from the ratios of cesium to ruthenium in Table 2, it is clear that a ratio higher than five is preferable, if it is assumed that the 5% loading of ruthenium has similar particle size.

To determine what ratio of cesium to ruthenium is optimal the particle size must be controlled better. Otherwise it is difficult to determine which effect is most important. This also means that the optimal loading of 1% ruthenium may be a combination of small better dispersed particles and more frequent contact between cesium and ruthenium. This is due to the limited surface exposure of the cesium ions, defined by the distribution of cesium in the crystal lattice of the cesium titanate. This scenario is also supported by the non-promoting effect observed by loading non-titanate cesium on the surface of the Ru-TiO$_2$ catalyst.

4 Conclusions

In conclusion, the synthesis of the nanostructured support materials $Na_2Ti_3O_7$, $K_2Ti_6O_{13}$, and $Cs_2Ti_6O_{13}$ from anatase TiO_2 nanoparticles has been performed. The produced nanostructured materials were loaded with ruthenium and tested in the ammonia decomposition reaction. The clear promoting effect of alkaline metals increasing in the sequence: Cs > K > Na was shown. Furthermore, a significant effect of the incorporation of the promoters in the support crystal lattice instead of classic surface promoting procedures was obtained. Further development of these Ru-titanate catalysts should also include long term stability measurement in the desired temperature interval.

Finally, the optimal apparent ruthenium loading on $Cs_2Ti_6O_{13}$ was found to be 1%, but further studies on the influence of the ruthenium particle size and the metal loading on the catalytic activities are needed, for this conclusion.

References

1. Dresselhaus M, Crabtree G, Buchanan M (2003) Basic research needs for a hydrogen economy. US Department of Energy, Washington, DC
2. Crabtree G, Dresselhaus M, Buchanan M (2004) Phys Today 57(12):39
3. Turner JA (2004) Science 305:972
4. Sun D, Srinivasan SS, Chen G, Jensen CM (2004) Rehydrogenation. J Alloy Compd 373(1–2):265
5. Furukawa H, Miller MA, Yaghi OM (2007) J Mater Chem 17:3197
6. Łodziana Z, Vegge T (2004) Phys Rev Lett 93:145501
7. Chłopek K, Frommen C, Leon A, Zabara O, Fichtner M (2007) J Mater Chem 17:3496
8. Vajo JJ, Skeith SL, Mertens F (2005) J Phys Chem B 109:3719
9. Lohstroh W, Fichtner M (2007) J Alloy Compd 332:446
10. Zûttel A (2003) Mater Today 6:24
11. Rostrup-Nielsen JR, Rostrup-Nielsen T (2002) Cattech 6:150
12. Clark WW II, Rifkin J (2006) Energy Policy 34:2630
13. Ni M, Leung DYC, Leung MKH, Sumathy K (2006) Fuel Process Technol 87:461
14. Saxe M, Alvfors P (2007) Energy 32:42
15. Ni M, Leung MKH, Leung DYC, Sumathy K (2007) Renew Sust Energy Rev 11:401
16. Neburchilov V, Martin J, Wang H, Zhang J (2007) J Power Sources 169:221
17. Delsman ER, Uju CU, de Croon MHJM, Schouten JC, Ptasinski KJ (2006) Energy 31:3300
18. Thomas G, Parks G (2006) Potential roles of ammonia in a hydrogen economy. US Department of Energy, Washington, DC
19. Zamfirescu C, Dincer I (2008) J Power Sources 185:459
20. Klerke A, Christensen CH, Nørskov JK, Vegge T (2008) J Mater Chem 18:2304
21. Sørensen RZ, Hummelshøj JS, Klerke A, Reeves JB, Vegge T, Nørskov JK, Christensen CH (2008) J Am Chem Soc 130:8660
22. Vegge T, Sørensen RZ, Klerke A, Hummelshøj JS, Johannessen T, Nørskov JK, Christensen CH (2008) Solid-state hydrogen storage: materials and chemistry. Woodhead Publishing LTD., England
23. Christensen CH, Sørensen RZ, Johannessen T, Quaade U, Honkala K, Elmøe TD, Køhler R, Nørskov JK (2005) J Mater Chem 15:4106
24. Christensen CH, Johannessen T, Sørensen RZ, Nørskov JK (2006) Catal Today 111:140
25. Hansen JB (1995) In: Nielsen A (ed) Ammonia, catalysis and manufacture. Springer, Heidelberg
26. Chellappa AS, Fisher CM, Thomson WJ (2002) Appl Catal A 227:231
27. Choudhary TV, Sivadinarayan C, Goodman DW (2001) Catal Lett 72:197
28. Ganley JC, Seebauer EG, Masel RI (2004) J. Power Sources 137:53–61
29. Raróg-Pilecka W, Szmigeel D, Kowalczyk Z, Jodis S, Zielinski J (2003) J Catal 218:465
30. Sørensen RZ, Nielsen LJE, Jensen S, Hansen O, Johannesen T, Quaade U, Christensen CH (2003) Catal Commun 6:229
31. Sørensen RZ, Klerke A, Quaade U, Jensen S, Hansen O, Christensen CH (2006) Catal Lett 112:77
32. Yin SF, Xub BQ, Zhou XP, Au CT (2004) Appl Catal A 277:1
33. Miao L, Ina Y, Tanemura S, Jiang T, Tanemura M, Kaneko K, Toh S, Mori Y (2007) Surf Sci 601:2792
34. Du GH, Chen Q, Peng L-M (2001) Appl Phys Lett 79:3702
35. Klitgaard SK, DeLaRiva AT, Helveg S, Werchmeister RM, Christensen CH (2008) Catal Lett 126:213
36. Chen Q, Zhou W, Du G, Peng L-M (2002) Adv Mater 14:1208
37. Du GH, Chen Q, Han PD, Yu Y, Peng L-M (2003) Phys Rev B 67:035323
38. Grey IE, Madsen IC, Watts JA, Bursill LA, Kwiakowska J (1985) J Solid State Chem 58:350
39. Masaki N, Uchida S, Sato T (2001) J Mater Chem 12:305
40. Wang SJ, Yin SF, Li L, Xu BQ, Ng CF, Au CT (2004) Appl Catal B Environ 52:287
41. Guraya M, Sprenger S, Rarog-Pilecka W, Szmigiel D, Kowalczyk Z, Muhler M (2004) Appl Surf Sci 238:77
42. Zhang J, Xu H, Ge Q, Li W (2006) Catal Commun 7:152
43. Sørensen RZ, Klerke A, Quaade U, Jensen S, Hansen O, Christensen CH Catal Lett 112 (206) 77